AGU PUBLICATIONS

JGR

Journal of Geophysical Research: Space Physics

RESEARCH ARTICLE
10.1002/2014JA020744

Key Points:
- Conditions at Neptune are the worst for magnetopause reconnection
- Reconnection site locations on Neptune's magnetopause are highly dynamic
- One polarity of the prevailing IMF is more favorable than the other at equinox

Correspondence to:
A. Masters,
a.masters@imperial.ac.uk

Citation:
Masters, A. (2015), Magnetic reconnection at Neptune's magnetopause, *J. Geophys. Res. Space Physics*, *120*, 479–493, doi:10.1002/2014JA020744.

Received 16 OCT 2014
Accepted 22 DEC 2014
Accepted article online 30 DEC 2014
Published online 29 JAN 2015

Magnetic reconnection at Neptune's magnetopause

A. Masters[1]

[1]Blackett Laboratory, Imperial College London, London, UK

Abstract What we know about the magnetosphere of the outermost planet, Neptune, is primarily based on data taken during the Voyager 2 flyby in 1989. Establishing how Neptune's magnetosphere interacts with the solar wind is crucial for understanding the dynamics of the system. Here we assess how magnetic reconnection couples the solar wind to Neptune's magnetosphere, using analytical modeling that was recently applied to the case of Uranus. The modeling suggests that typical near-Neptune solar wind parameters make conditions at Neptune's magnetopause less favorable for magnetic reconnection than at the magnetopause boundary of any other solar system magnetosphere. The location of reconnection sites on Neptune's magnetopause is expected to be highly sensitive to planetary longitude and season, as well as interplanetary magnetic field (IMF) orientation, which is similar to the situation at Uranus. Also similar to past Uranus results, the present Neptune modeling indicates a seasonal effect, where one of the two dominant (Parker spiral) IMF orientations produces more favorable conditions for magnetopause reconnection than the other near equinox. We estimate the upper limit of the reconnection voltage applied to Neptune's magnetosphere as 35 kV (the typical voltage is expected to be considerably lower). Further progress in understanding the solar wind-magnetosphere interaction at Neptune requires other coupling mechanisms to be considered, as well as how reconnection operates at high plasma β.

1. Introduction

Neptune is the outermost planet in our solar system. Much of what we know about this distant planetary system is based on data taken during a single spacecraft flyby, made by Voyager 2 in 1989 [*Stone and Miner*, 1989]. Neptune orbits the Sun at a distance ~30 times greater than the mean Sun-Earth distance (an Astronomical Unit, AU), and its axial tilt of 28.3° leads to strong seasons.

Like a number of other solar system planets, Neptune is protected from the solar wind by an intrinsic magnetic field [*Ness et al*., 1989]. Neptune's magnetic field is well represented as an offset tilted dipole, where the magnetic dipole and rotation axes subtend a relatively large angle of 47°, and the dipole center is displaced from the planet's center by 0.55 Neptune radii (R_N, 1 R_N = 24765 km) [*Ness et al*., 1989; *Connerney et al*., 1991; *Holme and Bloxham*, 1996]. The planetary magnetic field presents an obstacle to the solar wind, resulting in a magnetosphere that is similar to those that surround other magnetized planets in some respects [e.g., *Bagenal*, 2013]. However, Neptune's large dipole tilt leads to significant changes in the magnetic environment surrounding the planet over a Neptune day of 16.1 h, as illustrated in Figure 1. This results in a magnetosphere that undergoes dramatic diurnal reconfiguration [e.g., *Voigt and Ness*, 1990].

When Voyager 2 flew by Neptune in 1989, the spacecraft entered the magnetosphere via Neptune's magnetospheric cusp. The configuration of the system at this time is illustrated in Figure 1b (the spacecraft encountered the cusp close to the planet-Sun line). Voyager 2 then flew through the magnetosphere, resolved plasma populations closer to the planet that are likely sourced from Triton (Neptune's largest moon), and later exited through the distant flank of the system's magnetopause boundary [*Belcher et al*., 1989; *Ness et al*., 1989; *Richardson and McNutt*, 1990; *Mauk et al*., 1991; *Richardson et al*., 1991; *Szabo et al*., 1991; *Zhang et al*., 1991; *Lepping et al*., 1992; *Richardson*, 1993]. Partly due to the lack of dayside magnetopause observations, there has been little focus on the question of how Neptune's magnetosphere interacts with the solar wind, with the exception of *Selesnick* [1990], who considered plasma loss from the system due to solar wind-driven convection. The purpose of this paper is to resume detailed investigation of this interaction, by considering the operation of magnetic reconnection at Neptune's magnetopause.

The process of magnetic reconnection occurs at current layers across which there is some shear in the magnetic field. Reconnection changes the structure of the field and releases magnetic energy [*Dungey*, 1961].

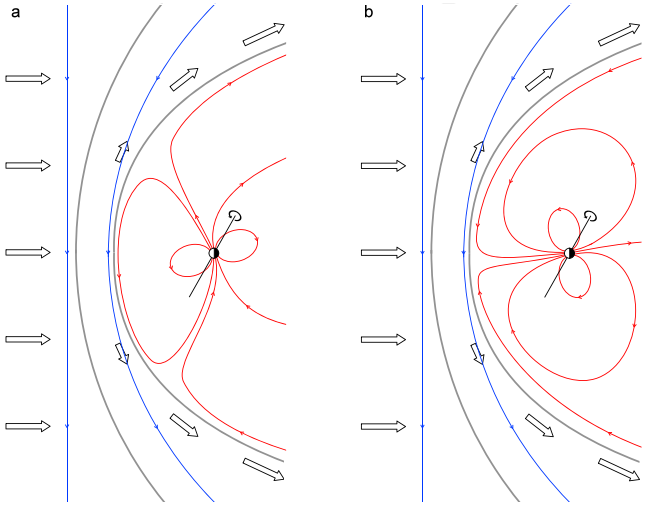

Figure 1. Diagrams illustrating Neptune's dynamic magnetosphere at northern winter solstice (the closest solstice or equinox to the Voyager 2 flyby that occurred in 1989). (a and b) Configurations of the system separated by half a planetary rotation, for the special case of southward interplanetary magnetic field (IMF) and no magnetic connection across the magnetopause boundary. In Figures 1a and 1b the solar wind plasma flow is indicated by block arrows, the IMF is shown in blue, Neptune's bow shock and magnetopause are shown as (outer and inner) gray curves, the planetary magnetic field is shown in red, and the planetary rotation axis is shown in black.

The magnetopause boundary of a planetary magnetosphere is an example of a current layer where reconnection can occur and allow solar wind energy into the system. Much of present understanding of reconnection is based on in situ observations of its operation at ~1 AU, at current sheets embedded in the solar wind, and at Earth's magnetopause (see the recent reviews by *Fuselier and Lewis* [2011], *Gosling* [2012], and *Paschmann et al*. [2013]). A thin current layer (order 1 ion inertial length) and both sub-Alfvénic relative particle drift and sub-Alfvénic flow shear in the direction of the reconnecting fields are thought to be required for reconnection to take place [*Sanny et al*., 1994; *Swisdak et al*., 2003, 2010; *Phan et al*., 2010, 2011, 2013; *Cassak and Otto*, 2011]. Once operating, the strength of the electric field resulting from reconnection is controlled by the magnetized plasma conditions in the adjacent environments [e.g., *Cassak and Shay*, 2007; *Mozer and Hull*, 2010] and a (dimensionless) reconnection efficiency that may be dependent on these local parameters [*Sonnerup*, 1970; *Slavin and Holzer*, 1979; *Anderson et al*., 1997; *DiBraccio et al*., 2013].

Desch et al. [1991] proposed that reconnection at Neptune's magnetopause drives the planet's radio emission, and *Huddleston et al*. [1997] discussed to what extent magnetopause reconnection leads to transport of solar wind plasma into Neptune's magnetosphere. Beyond these studies there has been very little discussion of this topic in the literature, and none based on current understanding of how magnetic reconnection works. In this paper we use an analytical modeling approach as the basis for applying this understanding to the case of Neptune's magnetopause. This allows us to examine how favorable typical conditions are for reconnection, where we expect reconnection to occur on the boundary under different conditions, and how strong we expect the resulting reconnection electric fields to be.

The magnetosphere of Neptune is often paired with that of Uranus, since they are similarly asymmetric and dynamic. An equivalent magnetopause reconnection assessment for Uranus (based on the same modeling approach) has recently been reported by *Masters* [2014]. At a number of points in the following sections we refer the reader to this companion Uranus publication, in order to limit reproduction of material. In addition, comparison between the present Neptune results and those of this past Uranus study is made during the discussion.

2. Approach

We use the Neptune Solar Orbital (NSO) coordinate system. The origin is at the center of Neptune, and the x axis points toward the Sun. The y axis defines an xy plane that lies in Neptune's orbital plane, and the y axis is antiparallel to the planet's orbital velocity vector. The z axis completes the right-handed orthogonal set, pointing north of the ecliptic. The terms "northward" and "southward" refer to the directions that are parallel and antiparallel to the z axis, respectively. The NSO coordinate system is the Neptune equivalent of Geocentric Solar Ecliptic (GSE) coordinates commonly employed in the case of Earth. However, due to Neptune's small orbital speed with respect to the near-Neptune solar wind speed, we apply no aberration to the NSO system (in contrast to the use of the GSE system at Earth).

Table 1. Fixed Solar Wind Conditions Upstream of Neptune's Bow Shock Used as Input to the Magnetopause Reconnection Modeling [*Slavin and Holzer*, 1981]

Flow Speed	450 km s^{-1}
Proton number density	0.02 cm^{-3}
Plasma pressure	1.6×10^{-5} nPa
Magnetic field strength	0.11 nT
Sonic Mach number	28
Alfvén Mach number	24

The analytical modeling approach used here is identical to that used by *Masters* [2014] in their assessment of reconnection at Uranus' magnetopause. To avoid reproduction of material, we refer the reader to this publication for full details of the approach. In this section we summarize the methodology and highlight Neptune-specific model inputs.

2.1. Treatment of Near-Magnetopause Parameters

Typical near-Neptune solar wind parameters are key inputs to the analytical modeling. These solar wind inputs can either be derived from the measurements made by Voyager 2 upstream of the planetary bow shock or from predictions based on present understanding of how solar wind parameters vary with heliocentric distance [e.g., *Slavin and Holzer*, 1981]. Note that the same choice must be made for the case of near-Uranus solar wind conditions, where the set of inputs is similar whichever source is chosen [*Masters*, 2014].

The same is not true of Neptune. Voyager 2 measurements at Neptune's dayside bow shock were presented by *Szabo and Lepping* [1995]. A number of the solar wind parameters measured upstream of Neptune's bow shock differ significantly from the predicted (typical) values. Most strikingly, the measured upstream proton number density of 0.0046 cm^{-3} at Neptune is lower than the predicted value by a factor of ~4 [e.g., *Slavin and Holzer*, 1981]. However, this difference is not surprising, given the level of solar wind variability. In the present study we require typical solar wind conditions in order to draw qualitative conclusions about the general nature of reconnection at Neptune's magnetopause. As a result, we choose to use solar wind scaling predictions as inputs, rather than values based on the Voyager 2 "snapshot" of dynamic solar wind conditions.

Fixed upstream solar wind inputs to the Neptune modeling are given in Table 1 [e.g., *Slavin and Holzer*, 1981], where the solar wind plasma flow is antisunward. The influence of interstellar pickup ions is not considered (see discussion in section 4.1). The orientation of the interplanetary magnetic field (IMF) is set as a free parameter but is constrained to lie in the *yz* plane. This constrained range of IMF orientations captures the two prevailing IMF orientations at Neptune orbit (see section 3) and simplifies our modeling of Neptune's magnetosheath (the solar wind downstream of the bow shock) [e.g., *Petrinec et al*., 2003]. A neutral solar wind plasma with an ion composition of 96% protons and 4% He^{++} by number is assumed when calculating mass densities.

To describe the dayside surface of both Neptune's bow shock and magnetopause, we use parabolic conic sections, with standoff distances of 32 and 25 R_N, respectively [*Ness et al*., 1989]; the focus of both of which is located on the *x* axis, halfway between the center of the planet and the magnetopause. Both the bow shock and magnetopause surfaces are axisymmetric about the *x* axis.

Maps of magnetized plasma parameters immediately adjacent to the model Neptune magnetopause surface are the basis of our approach. For external, magnetosheath, solar wind conditions we follow four steps. First, we specify all plasma parameter maps using expressions based on a hydrodynamic treatment of solar wind flow around a magnetospheric obstacle [*Petrinec and Russell*, 1997]. Second, we specify draped IMF vectors using expressions presented by *Petrinec et al*. [2003] (based on the work of *Kobel and Flückiger* [1994]). Third, we include the effect of a typical plasma depletion layer (PDL) in the near-magnetopause magnetosheath [e.g., *Zwan and Wolf*, 1976] by lowering the mass density and raising the magnetic field strength at all points so as to reduce the local ratio of plasma to magnetic pressure (the plasma β) by 85% (without changing the total pressure). Finally, we correct for the influence of the draped IMF on the magnetosheath flow using the approach outlined by *Petrinec et al*. [1997].

For magnetospheric conditions immediately inside Neptune's magnetopause surface, we first assume that the local magnetospheric plasma pressure is equal to zero [e.g., *Belcher et al*., 1989]. The magnetospheric magnetic field is then determined by taking a specified orientation of the planetary dipole moment axis (controlled by the free parameters of Neptune season and Neptune longitude), calculating the planetary magnetic field at all points on the model magnetopause surface, setting all boundary normal field

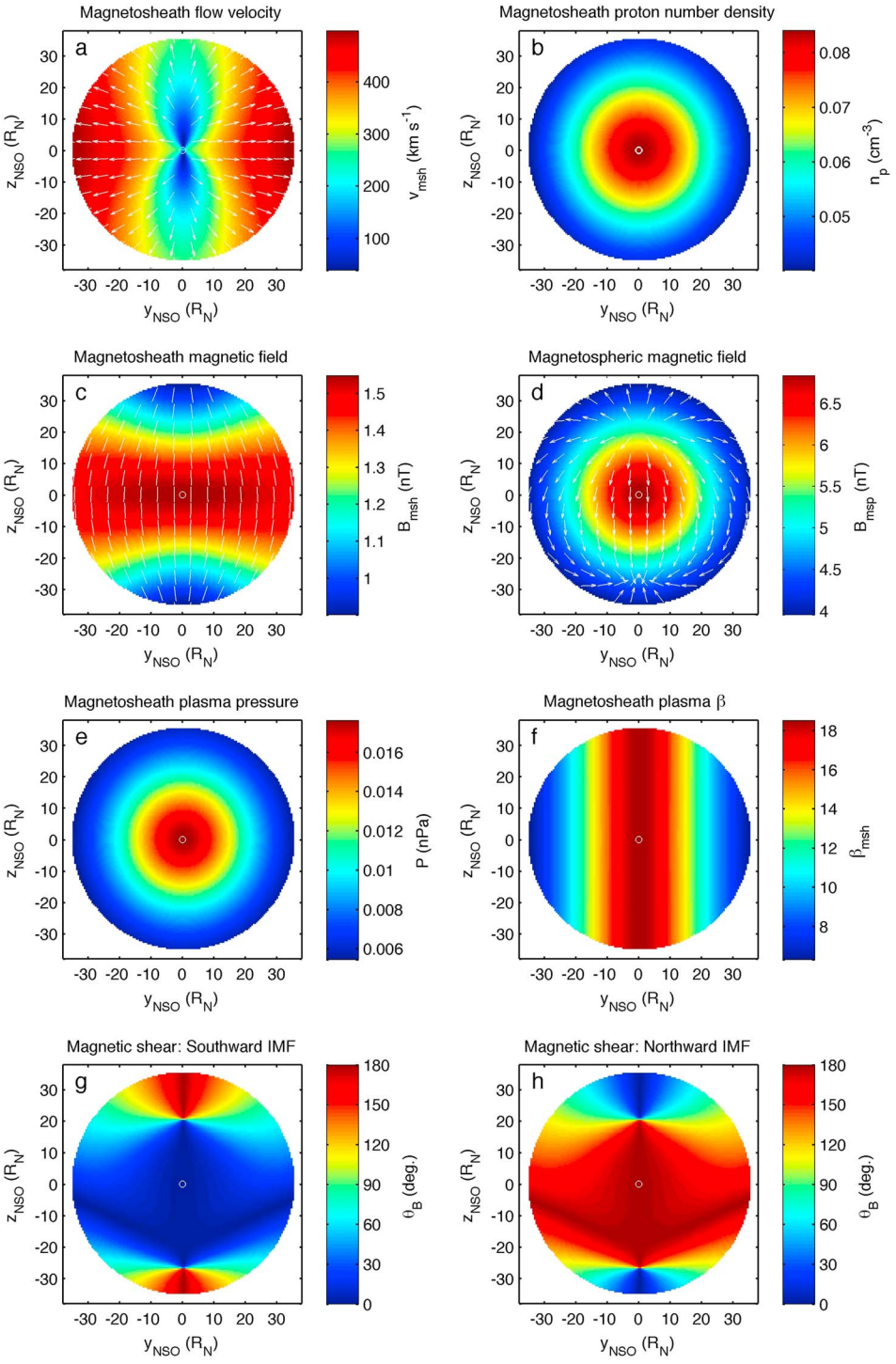

Figure 2. An example of model-predicted conditions at Neptune's magnetopause. (a) Magnetosheath plasma flow velocity. (b) Magnetosheath proton number density. (c) Magnetosheath magnetic field. (d) Magnetospheric magnetic field. (e) Magnetosheath plasma pressure. (f) Magnetosheath plasma β. (g) Cross-magnetopause magnetic shear for southward IMF. (h) Cross-magnetopause magnetic shear for northward IMF. Arrows give only the direction of vector fields (no arrow heads are shown in Figure 2c since both southward and northward IMFs are considered). In Figures 2a–2h the dayside magnetopause surface is viewed from along the upstream solar wind flow direction, and the circle centered on the origin represents the planet.

components to zero, and then specifying the local field strength as a value that achieves total pressure balance with the adjacent magnetosheath environment.

The free parameters in this modeling are the IMF orientation (in the *yz* plane), Neptune season, and phase of Neptune rotation (the time of day). For any combination of these free parameters the model gives maps of near-magnetosheath and near-magnetosphere conditions at Neptune's magnetopause.

2.2. Example Near-Magnetopause Parameters

To provide examples of near-magnetopause conditions given by the present modeling, we can specify free model parameters that reproduce the situation shown in Figure 1a. This requires a purely southward IMF, a Neptune season of exactly northern winter solstice, and a Neptune longitude that makes the planetary dipole axis lies in the *xz* plane, with a positive projection on the *x* axis. Note that this southward IMF orientation is rare but is used here to be consistent with the two-dimensional diagram shown in Figure 1a. The dominant IMF orientations are considered in section 3.

Figures 2a–2g show model-predicted conditions at Neptune's magnetopause for this combination of free parameters, all viewed from along the upstream solar wind flow (i.e., viewed from the Sun), and all showing only the dayside magnetopause surface. Figure 2a shows the magnetosheath flow velocity, where the influence of the draped IMF has been accounted for (see section 2.1). Figure 2b shows the magnetosheath proton number density, and Figure 2c shows the magnetosheath magnetic field. Figure 2d shows Neptune's magnetospheric magnetic field, where cusp features are in locations similar to those shown in Figure 1a, Figure 2e shows the plasma pressure in Neptune's magnetosheath, and Figure 2f shows the plasma β in the near-magnetopause magnetosheath. Figure 2g shows the angular difference between the magnetosheath and magnetospheric magnetic fields (the magnetic shear) across the model magnetopause surface.

If we reverse the direction of the IMF from southward to northward, this has no effect on Figures 2a–2f, except that the direction of the draped IMF in Figure 2c is reversed. This example can therefore also cover the combination of free model parameters where the IMF is northward (with other free parameters unchanged). Like southward IMF, a northward IMF orientation is rare (see section 3). Figure 2h shows the map of magnetic shear for northward IMF, which produces close to antiparallel magnetic fields over a larger fraction of the model magnetopause surface.

2.3. Example Magnetopause Reconnection Assessments

For the example conditions near Neptune's magnetopause presented in Figure 2, we can carry out example magnetopause reconnection assessments. When carrying out all such assessments, we consider a system where there is no magnetic connection across the magnetopause (i.e., a "closed" system) and assume that the magnetopause current sheet is sufficiently thin for reconnection everywhere on the surface [*Phan et al*., 2013]. A reconnection assessment then involves the separate application of two established conditions for reconnection onset, one concerning the drift of the potential reconnection site caused by the relative particle drift within the current layer (the diamagnetic drift condition) [*Swisdak et al*., 2003, 2010; *Phan et al*., 2010, 2013], and the other concerning the flow shear across the potential reconnection site (the flow shear condition) [*Cassak and Shay*, 2007; *Cassak and Otto*, 2011].

The diamagnetic drift condition places a lower limit on the magnetic shear at which reconnection can occur for a given level of current layer symmetry [*Swisdak et al*., 2010]. The level of asymmetry is quantified as the absolute difference between the plasma β on either side of the layer ($\Delta\beta$). The lower limit of magnetic shear increases with increasing $\Delta\beta$, restricting reconnection to closer to antiparallel magnetic fields (antiparallel reconnection cannot be suppressed by this effect). In the present modeling, the plasma β in Neptune's near-magnetopause magnetosheath is equal to $\Delta\beta$, and the model-predicted plasma β is high enough to require shears of greater than ~175° for reconnection onset at any point. The flow shear onset condition requires that the flow shear across the magnetopause current layer in the direction of reconnection outflow [*Swisdak and Drake*, 2007] must be lower than the outflow speed [*Cassak and Shay*, 2007] for onset to occur [*Cassak and Otto*, 2011].

Figures 3a–3c show the reconnection assessment results for the southward IMF case discussed in section 2.2 (see Figure 2a–2g). Dashed contours indicate where the transition from sub-Alfvénic to super-Alfvénic magnetosheath flow occurs. In Figure 3a the diamagnetic drift condition is applied and is only satisfied in the

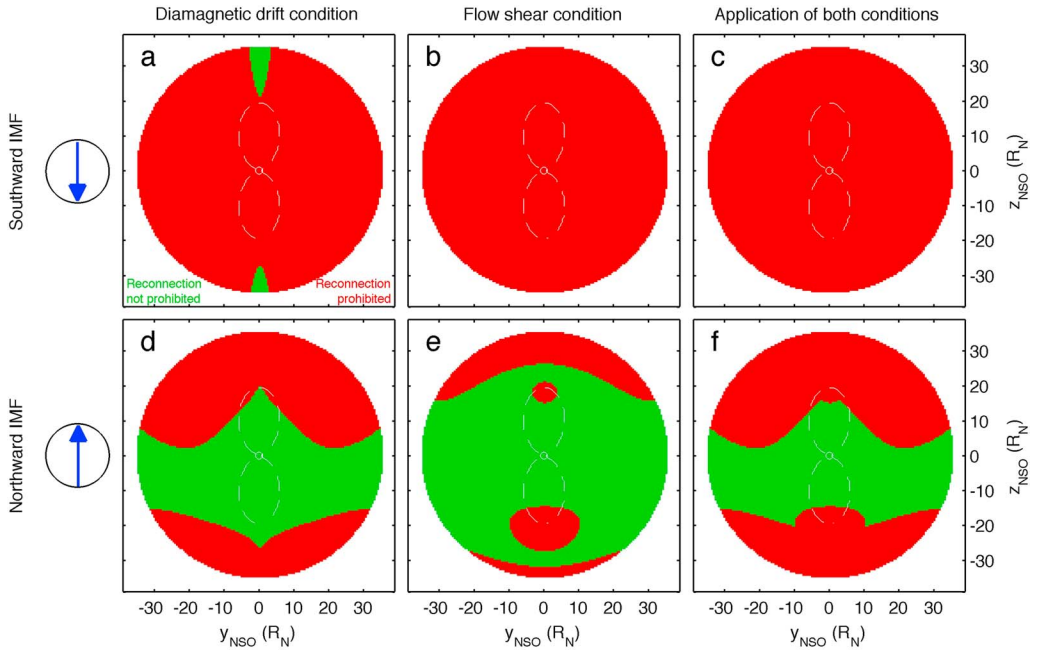

Figure 3. Example assessments of magnetic reconnection at Neptune's magnetopause. Panels in the same row correspond to the same IMF orientation, indicated by the far left circles that show the upstream IMF vector (with length 2 Neptune radii) projected onto the planet, as viewed from along the upstream solar wind flow direction. (a and d) The applications of the diamagnetic drift condition for reconnection onset. (b and e) The applications of the flow shear condition for reconnection onset. (c and f) The application of both onset conditions (requiring both conditions to be satisfied for reconnection to not be prohibited). In Figures 3a–3f the dayside magnetopause surface is viewed from along the upstream solar wind flow direction, the circle centered on the origin represents the planet, and the dashed contour bounds the region where the local magnetosheath flow is sub-Alfvénic. Regions of the surface shown in green indicate where the applied reconnection onset condition(s) is satisfied, and thus reconnection is not prohibited by the considered effect(s); whereas regions shown in red indicate where the condition(s) is not satisfied, and thus reconnection is prohibited by the considered effect(s).

regions of close to antiparallel magnetic fields (see Figure 2g) that are antisunward of the cusps. In Figure 3b the flow shear condition is applied and is not satisfied anywhere on the dayside boundary. Figure 3c applies both conditions, producing a total reconnection onset assessment that predicts that reconnection cannot occur anywhere on the dayside magnetopause for this combination of free parameters.

Figures 3d–3f show the reconnection assessment results for the northward IMF case discussed in section 2.2 (see Figures 2a–2f and 2h). These results differ significantly from the southward IMF case. Figure 3c shows that the large magnetic shear across the model surface leads to the satisfaction of the diamagnetic drift condition over a far larger region. Figure 3e shows that the flow shear condition is satisfied over the majority of the surface. Note that the location of regions where reconnection is (and is not) prohibited in Figure 3e (and Figure 3b) is not only controlled by the magnetosheath flow but also by how the expected reconnection outflow direction changes across the surface [*Swisdak and Drake*, 2007]. It is also worth pointing out that the reconnection outflow speed differs from the magnetosheath Alfvén speed [*Cassak and Shay*, 2007]. Figure 3f applies both conditions and predicts that reconnection onset is possible in a region that spans Neptune's dayside magnetopause.

At this point we remind the reader that a more comprehensive discussion of the present modeling approach can be found in *Masters* [2014]. This includes a more detailed description of how these reconnection onset conditions are applied.

3. Results: Solstice and Equinox

In sections 2.2 and 2.3 we presented examples of how the present analytical modeling can be used to predict where reconnection onset will occur at Neptune's magnetopause. In these examples we considered only two

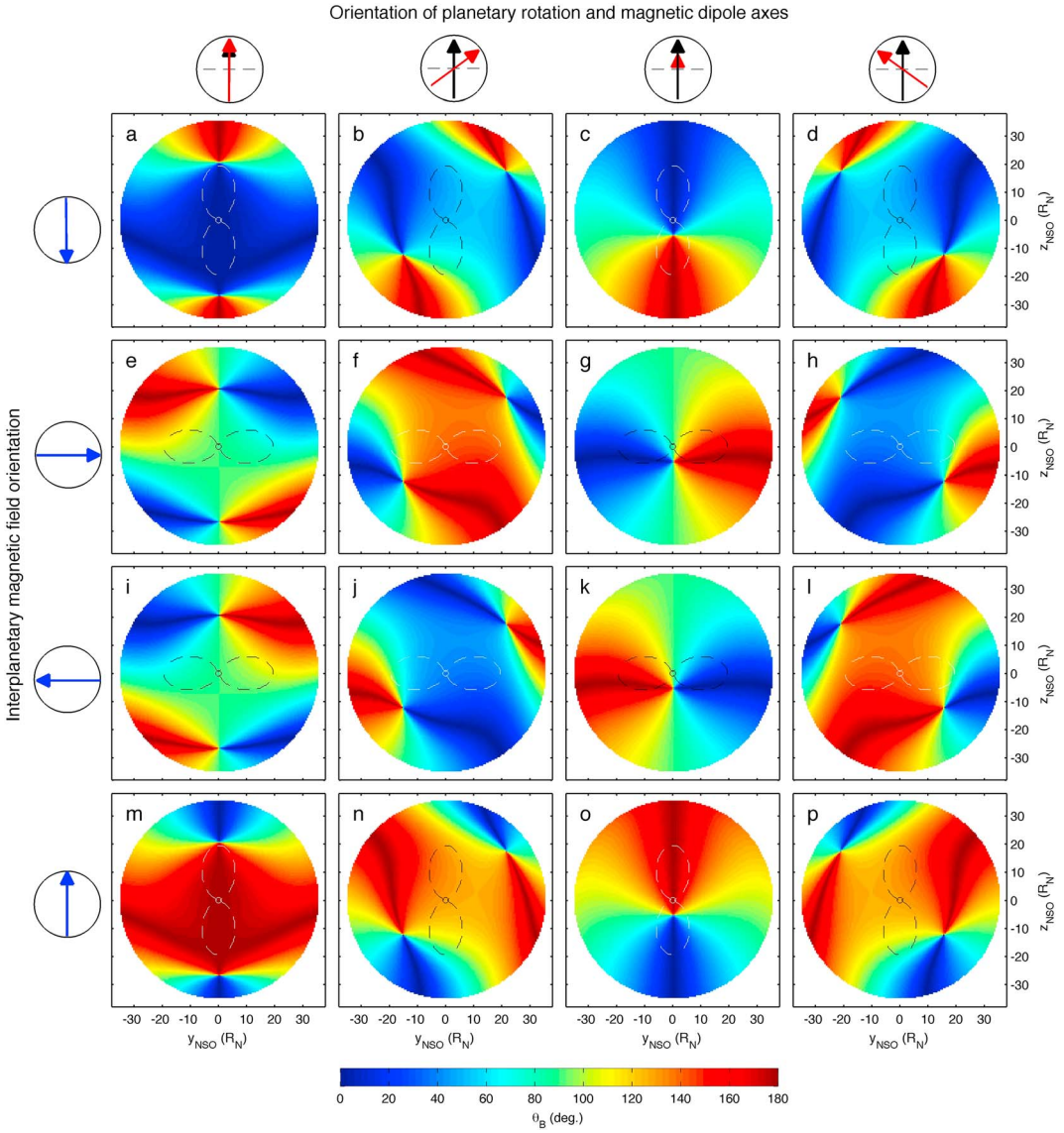

Figure 4. (a–p) The variable magnetic shear across Neptune's magnetopause at northern winter solstice (the era of the 1989 flyby by Voyager 2). Panels in the same row correspond to the same IMF orientation, indicated by the far left circles that show the upstream IMF vector (with length 2 Neptune radii) projected onto the planet, as viewed from along the upstream solar wind flow direction. Panels in the same column correspond to the same orientation of planetary rotation and magnetic dipole axes, similarly shown in black and red (respectively) above each column. In Figures 4a–4p the magnetic shear across the dayside magnetopause is shown as viewed from along the upstream solar wind flow direction, the circle centered on the origin represents the planet, and the dashed contour bounds the region where the local magnetosheath flow is sub-Alfvénic.

IMF orientations, both at northern winter solstice and at the same planetary longitude. In this section we consider solstice and equinox conditions over a broader free parameter space.

Let us first extend our consideration of northern winter solstice on Neptune, since this is the closest solstice or equinox to the Voyager 2 flyby that took place in 1989. Figure 4 shows the magnetic shear across Neptune's magnetopause for 16 different pairings of IMF orientation and planetary longitude, all at northern winter solstice. Panels in the same row correspond to the same IMF orientation (illustrated to the left of each row), and panels in the same column correspond to the same Neptune longitude (i.e., the same orientation of magnetic dipole axis with respect to the planetary rotation axis, illustrated above each column). The following four different IMF orientations are considered: Purely southward IMF (Figures 4a–4d), IMF parallel to the *y* axis (Figures 4e–4h), IMF antiparallel to the *y* axis (Figures 4i–4l), and purely northward IMF (Figures 4m–4p). Figures 4a,

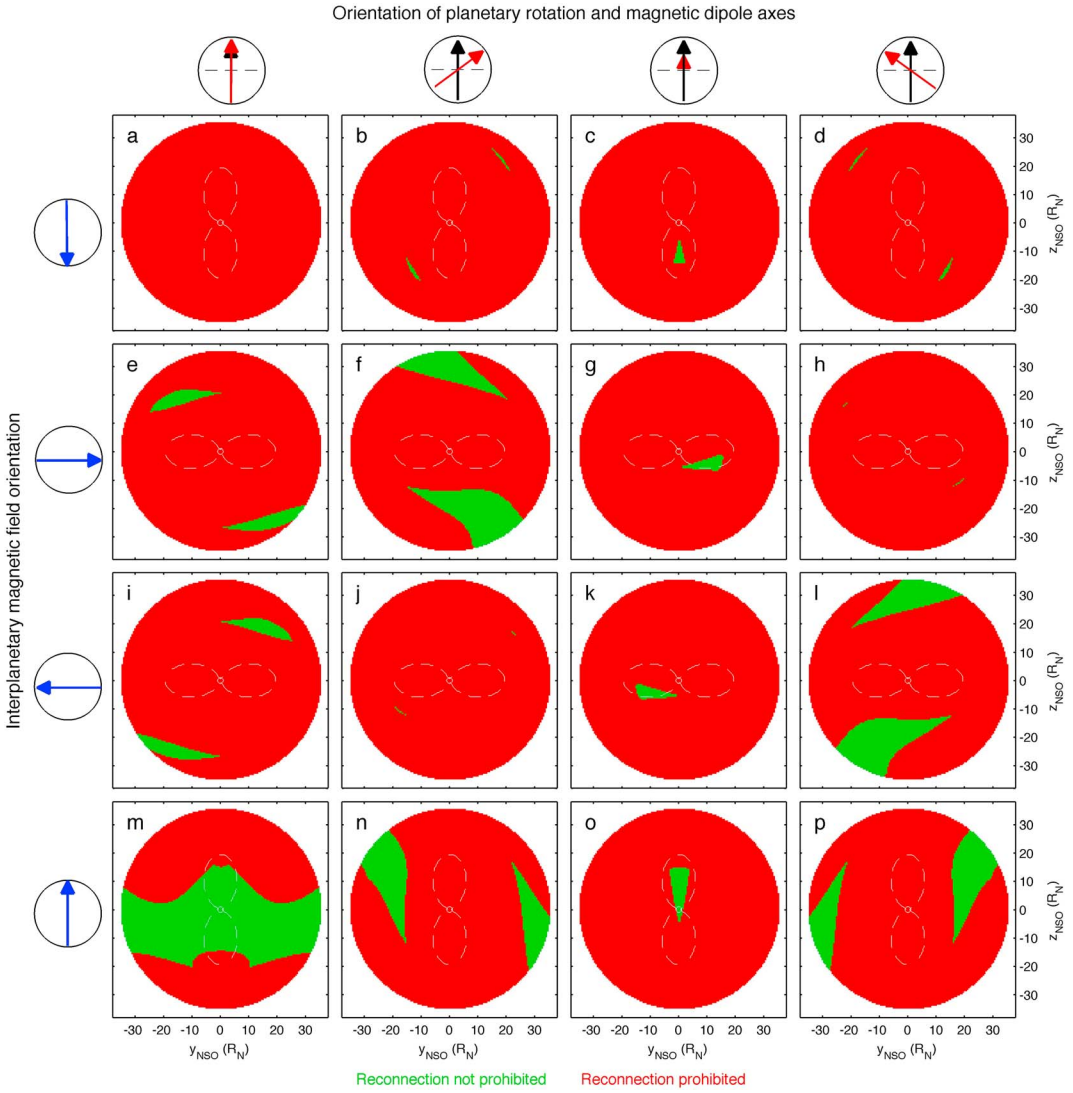

Figure 5. (a–p) Assessments of magnetic reconnection at Neptune's magnetopause at northern winter solstice (the era of the 1989 flyby by Voyager 2). Panels in the same row correspond to the same IMF orientation, indicated by the far left circles that show the upstream IMF vector (with length 2 Neptune radii) projected onto the planet, as viewed from along the upstream solar wind flow direction. Panels in the same column correspond to the same orientation of planetary rotation and magnetic dipole axes, similarly shown in black and red (respectively) above each column. In Figures 5a–5p the dayside magnetopause is shown as viewed from along the upstream solar wind flow direction, both the reconnection site drift and flow shear conditions for reconnection onset have been applied (green: reconnection not prohibited; red: reconnection prohibited), the circle centered on the origin represents the planet, and the dashed contour bounds the region where the local magnetosheath flow is sub-Alfvénic.

4e, 4i, and 4m correspond to the same dipole axis orientation as the examples given in section 2, and in subsequent columns the dipole axis is rotated about the planetary rotation axis in increments of 90° (in the sense of Neptune's rotation). The magnetic shear map for the southward IMF example presented in section 2.2 (Figure 2g) is shown in Figure 4a, and the northward IMF example (Figure 2h) is shown in Figure 4m. In all panels the region of the dayside magnetopause surface where the adjacent magnetosheath flow is sub-Alfvénic is the region bounded by the dashed contours.

We expect an IMF that is close to parallel or antiparallel to the *y* axis to be the dominant orientation at Neptune's orbit [*Parker*, 1958], so Figures 4e–4l show the most frequent IMF orientations, although rarer northward/southward orientations should be possible. The magnetic shear across Neptune's magnetopause at solstice is highly variable and controlled by planetary longitude, as well as the variable orientation of the

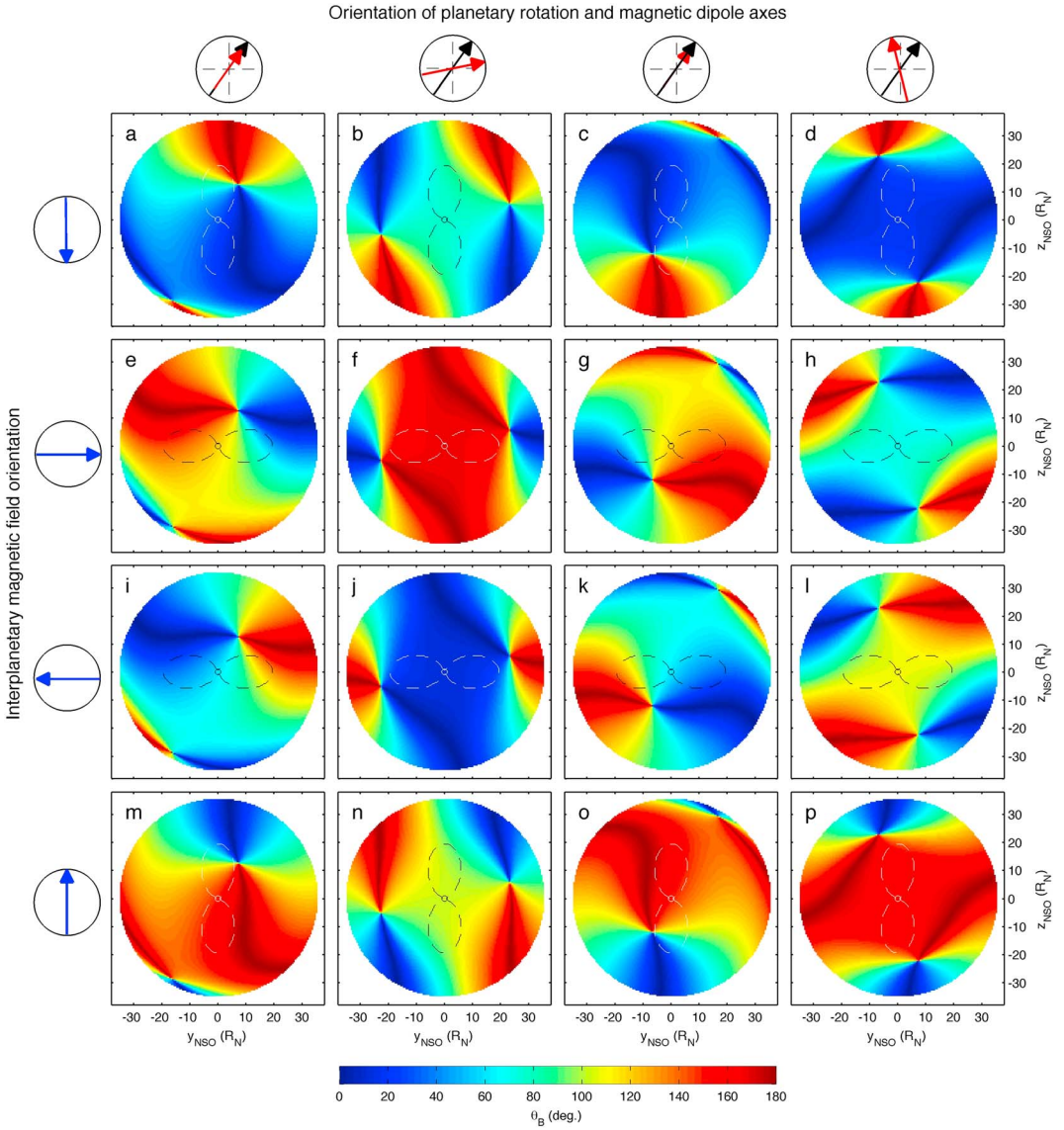

Figure 6. (a–p) The variable magnetic shear across Neptune's magnetopause at northern spring equinox (28 February 2038). Panels in the same row correspond to the same IMF orientation, indicated by the far left circles that show the upstream IMF vector (with length 2 Neptune radii) projected onto the planet, as viewed from along the upstream solar wind flow direction. Panels in the same column correspond to the same orientation of planetary rotation and magnetic dipole axes, similarly shown in black and red (respectively) above each column. In Figures 6a–6p the magnetic shear across the dayside magnetopause is shown as viewed from along the upstream solar wind flow direction, the circle centered on the origin represents the planet, and the dashed contour bounds the region where the local magnetosheath flow is sub-Alfvénic.

IMF. The corresponding total magnetopause reconnection assessment (equivalents of Figures 3c and 3f) for each panel in Figure 4 is shown in Figure 5. These plots indicate that reconnection will be suppressed over the majority of Neptune's dayside magnetopause in almost all cases, and in all cases of the prevailing IMF orientations (Figure 5e–5l). These results are qualitatively the same for northern summer solstice.

Let us now consider northern spring equinox on Neptune, which will occur on 28 February 2038. Figure 6 shows equinox magnetic shear maps for a range of IMF orientations and planetary longitudes, in the same format as Figure 4. Like Figure 4, Figure 6 also shows a variable magnetic shear across the dayside magnetopause that is controlled by both planetary longitude and IMF orientation. However, there appears to be a typically higher magnetic shear across the subsolar region (close to the *x* axis) for one of the dominant IMF polarities (Figures 6e–6h) than for the other dominant polarity (Figures 6i–6l). Figure 7 shows full

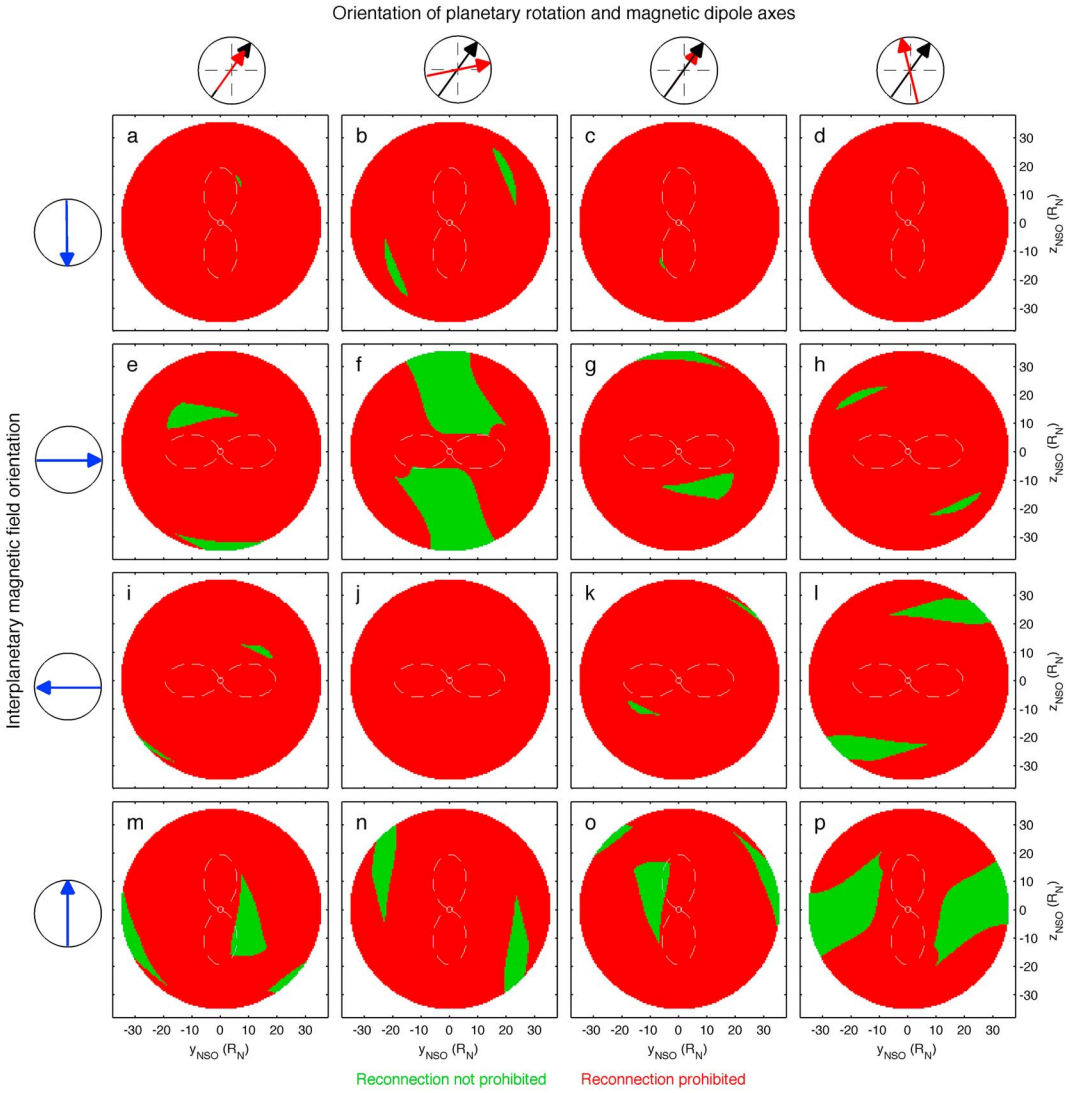

Figure 7. (a–p) Assessments of magnetic reconnection at Neptune's magnetopause at northern spring equinox (28 February 2038). Panels in the same row correspond to the same IMF orientation, indicated by the far left circles that show the upstream IMF vector (with length 2 Neptune radii) projected onto the planet, as viewed from along the upstream solar wind flow direction. Panels in the same column correspond to the same orientation of planetary rotation and magnetic dipole axes, similarly shown in black and red (respectively) above each column. In Figures 7a–7p the dayside magnetopause is shown as viewed from along the upstream solar wind flow direction, both the reconnection site drift and flow shear conditions for reconnection onset have been applied (green: reconnection not prohibited; red: reconnection prohibited), the circle centered on the origin represents the planet, and the dashed contour bounds the region where the local magnetosheath flow is sub-Alfvénic.

reconnection assessments for equinox, where each panel is paired with the equivalent panel in Figure 6. As for solstice, these equinox assessments predict that reconnection onset cannot take place over the majority of the dayside magnetopause surface in almost all cases. The difference between IMF polarities at equinox that we noted in Figure 6 is also apparent in Figure 7, where the suppression of reconnection onset is more severe for the polarity with lower magnetic shear across the subsolar region (Figures 7i–7l, cf. Figures 7e–7h). These results are qualitatively the same for northern fall equinox.

4. Discussion

Because we have followed the same modeling approach as *Masters* [2014], these results concerning reconnection at Neptune's magnetopause can be directly compared to equivalent Uranus results. The Uranus

and Neptune results are similar in that they both predict a highly variable cross-magnetopause magnetic shear for all seasons, with planetary longitude playing an important role. In addition, typical suppression of reconnection across the majority of the dayside magnetopause is common to both the ice giant planets, and there are similar indications of a seasonal effect.

The following subsections cover specific discussion topics, focusing on the comparison between magnetopause reconnection at Uranus and Neptune in order to highlight the predicted differences. To avoid reproduction of material, discussion points concerning our (idealized) modeling approach (which are thus common to both the past Uranus and present Neptune studies) are not included here, and we refer the reader to *Masters* [2014] where these issues are considered.

4.1. The Influence of Near-Neptune Solar Wind Conditions

Masters [2014] discussed how increasing solar wind Mach numbers with heliocentric distance are expected to make magnetosheath conditions at Uranus less favorable for magnetopause reconnection than at the magnetopause of any of the magnetized planet closer to the Sun. The physics underlying this argument is that higher upstream Mach numbers produce a higher downstream plasma β in the planetary magnetosheath and super-Alfvénic magnetosheath flow adjacent to a greater fraction of the dayside magnetopause surface. These changes in magnetosheath environment with solar wind Mach numbers suggest that there is both greater diamagnetic drift suppression of reconnection (i.e., onset becomes increasingly restricted to regions of close to antiparallel magnetic fields) and greater flow shear suppression of reconnection at the magnetopauses of planets that orbit the Sun at larger distances.

This argument can be extended to Neptune. Solar wind Mach numbers are slightly higher at Neptune orbit than at Uranus orbit (the Alfvén Mach number at Neptune is ~24 compared to ~23 at Uranus) [*Slavin and Holzer*, 1981; *Bagenal et al*., 1987]. This suggests that conditions at Neptune's magnetopause are less favorable for reconnection than at any other planetary magnetopause in the solar system. This expectation is consistent with the present Neptune results, where the model-predicted magnetosheath plasma β at Neptune's magnetopause is slightly higher than at Uranus (maximum value of ~18 in Figure 2f, compared to ~16 at Uranus), which means that magnetopause reconnection is generally restricted to slightly higher magnetic shears at Neptune than at Uranus ($>$175° at Neptune's magnetopause compared to $>$170° at Uranus'). Also, the fraction of Neptune's dayside magnetopause where the nearby magnetosheath flow is sub-Alfvénic is slightly smaller than in the case of Uranus. In addition, at some sufficiently high solar wind Alfvén Mach number, we expect the level of the magnetosheath PDL to be lower; i.e., we expect the PDL to cause a smaller reduction in the local plasma β. Since the solar wind Alfvén Mach number at ~30 AU is higher than at any other planet, it is possible that the typical PDL at Neptune is "weaker" than we have assumed in our modeling (see section 2.1). If so, this would reinforce the conclusions drawn here.

However, while modeling results support the statement that typical conditions at Neptune's magnetopause are less favorable for reconnection than those at Uranus, the predicted differences between the two planets are marginal. Changes in the solar wind (influenced by the solar cycle) will likely make it difficult to resolve such a small distinction using future in situ observations.

The near-Neptune solar wind conditions used as model inputs in this study (see Table 1) do not consider the influence of interstellar pickup ions, the acceleration of which accounts for a significant fraction of the energy dissipated at the solar wind termination shock [e.g., *Decker et al*., 2008]. The justification for this is the analysis of Voyager 2 observations at Neptune's bow shock reported by *Szabo and Lepping* [1995]. These authors showed that the in situ data are in good agreement with shock jump conditions, suggesting that the situation at Neptune's bow shock is unlike that at the termination shock in the more distant heliosphere. If a dynamically significant population of nonthermal pickup ions were present at 30 AU, then we also might expect this to reinforce the conclusions of the present study.

4.2. Seasonal Effects

The equivalent Uranus results presented by *Masters* [2014] suggest a seasonal dependence of magnetopause reconnection. The modeled magnetic shear across the subsolar Uranian magnetopause at solstice varies similarly for both the prevailing IMF orientations over a Uranus rotation, whereas at equinox one produces typically higher subsolar shears than the other. This difference is reflected in the daily changes in the fraction of the dayside Uranian magnetopause where reconnection onset conditions are met. At solstice there is

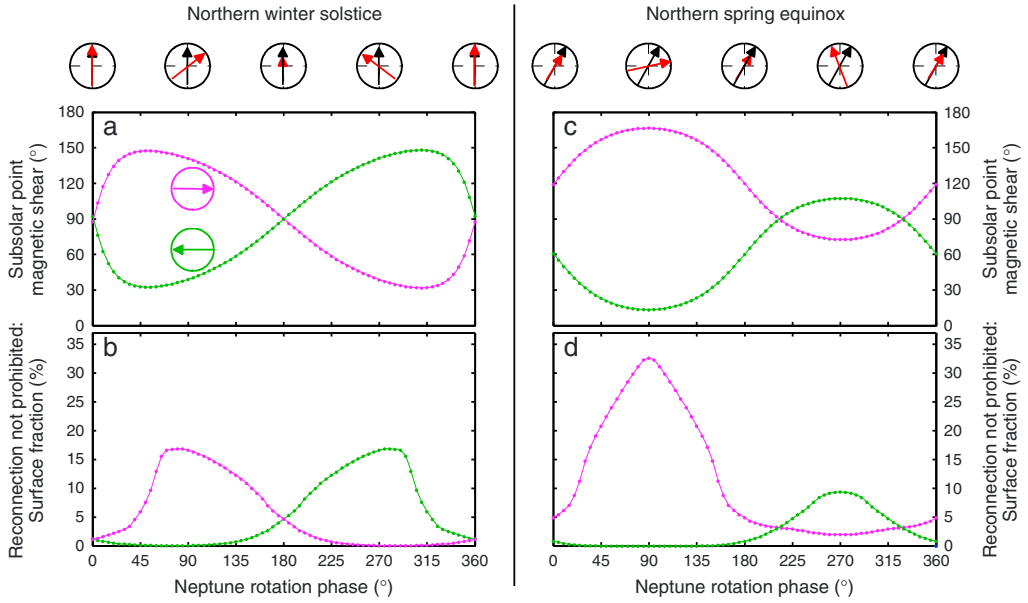

Figure 8. An assessment of seasonal influences on reconnection at Neptune's magnetopause. (a) Variation of the magnetic shear across the magnetopause subsolar point over a Neptune day, at northern winter solstice. (b) Variation of the percentage of the dayside magnetopause surface area where reconnection onset is not prohibited over a Neptune day, at northern winter solstice. (c) Variation of the magnetic shear across the magnetopause subsolar point over a Neptune day, at northern spring equinox. (d) Variation of the percentage of the dayside magnetopause surface area where reconnection onset is not prohibited over a Neptune day, at northern spring equinox. In Figures 8a and 8c the planetary rotation and magnetic dipole axes are shown (black and red, respectively, both with length 2 Neptune radii), projected onto the planet as viewed from along the upstream solar wind flow direction. The axes are shown at 90° increments of planetary rotation phase. In Figures 8a–8d the variation for a fixed IMF parallel to the *y* axis is shown in pink, and the variation for a fixed IMF antiparallel to the *y* axis is shown in green.

symmetry between the two IMF polarities, but this symmetry is broken at equinox, and the average fraction (over a Uranus rotation, considering both IMF polarities) appears to be lower at equinox than at solstice. The physical reason for this is the different allowed range of planetary dipole axis orientations at Uranian solstice compared to at equinox.

The present Neptune results also suggest a seasonal effect. Figure 8 explores this further. Figures 8a and 8b correspond to northern winter solstice (considered in Figures 4 and 5), whereas Figures 8c and 8d correspond to northern spring equinox (considered in Figures 6 and 7). Figures 8a and 8c show how the magnetic shear across the subsolar point on the model magnetopause (where the *x* axis intersects the surface) changes over a Neptune day for each season, and Figures 8b and 8d show how the fraction of the dayside magnetopause surface where reconnection onset is not prohibited also changes over a Neptune day for each season. Both of the dominant IMF orientations at Neptune are considered in all panels (note that the prevailing IMF orientations at Uranus and Neptune are essentially identical) [*Parker*, 1958].

The differences between Neptune seasons noted in section 3 are clear in Figure 8. The subsolar magnetic shear for both IMF polarities varies over a range of $<180°$ at both solstice and equinox. At solstice this range is the same for the two dominant IMF orientations, whereas at equinox the ranges only partially overlap (i.e., subsolar shear is generally higher for one than for the other). Fractions of the magnetopause surface where reconnection is not prohibited tend to be higher when the subsolar shear is higher, and at solstice there is symmetry between the two IMF polarities, as expected. However, at equinox the fraction reaches far higher values for one polarity than for the other, over the course of a Neptune day. The physical origin of these features and seasonal differences is the same as that invoked in the case of Uranus: Different ranges of possible dipole axis orientations at different seasons. A difference between the equivalent Uranus and Neptune seasonal assessments is that at Neptune the average fraction of the magnetopause surface where reconnection onset can occur (averaged over a Neptune day, considering both IMF polarities) is similar at solstice and equinox, whereas at Uranus the average values differ.

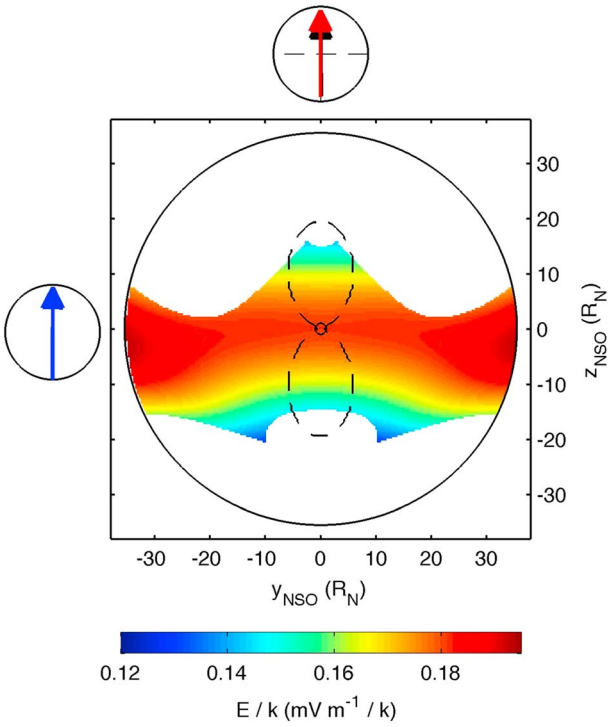

Figure 9. An assessment of the reconnection electric field strength at Neptune's magnetopause. A specific set of conditions is considered (shown in Figures 4m and 5m), corresponding to northern winter solstice. The circle to the left of the main panel shows the upstream IMF orientation, by projecting an IMF vector with length 2 Uranus radii onto the planet, as viewed from along the upstream solar wind flow direction. The circle above the main panel similarly shows the orientation of the planetary rotation and magnetic dipole axes, in black and red, respectively. In the main panel the dayside magnetopause is shown as also viewed along the upstream solar wind flow direction, the circle centered on the origin represents the planet, and the dashed contour bounds the region where the local magnetosheath flow is sub-Alfvénic. The color scale indicates what the ratio of the reconnection electric field strength to the dimensionless reconnection efficiency would be if onset were to occur. Color is only applied to regions of the surface where both reconnection onset conditions are satisfied (see Figure 5m).

4.3. Reconnection Electric Fields and the Reconnection Voltage

To understand to what extent the solar wind drives Neptune's magnetosphere, we need to constrain the reconnection voltage, and how this quantity varies with changing solar wind conditions, Neptune longitude, and Neptune season. This voltage is equivalent to the rate of open magnetic flux production resulting from reconnection. Note that plasma production inside Neptune's magnetosphere by the moon Triton may represent an internal driver of magnetospheric dynamics that competes with external driving by the solar wind [e.g., *Richardson*, 1993].

Our Neptune results allow us to begin to constrain the reconnection voltage applied to the system, by calculating an upper limit. The foundation of this is the determination of the electric field tangential to Neptune's magnetopause that would result from the onset of reconnection at some point—the reconnection electric field. This can be calculated using the near-magnetopause parameters that are treated by our modeling approach, based on an assumed value of the dimensionless reconnection efficiency [*Cassak and Shay*, 2007]. Figure 9 shows the magnetopause reconnection assessment for northern winter solstice and purely northward IMF shown in Figures 2h, 3d–3f, 4m, and 5m. This is the assessment where reconnection is possible over the greatest fraction of the modeled dayside magnetopause surface. In Figure 9 the reconnection electric field strength divided by the reconnection efficiency is shown in the region of the surface where reconnection is not prohibited.

There is some debate about how the reconnection efficiency depends on local parameters. Some authors argue that the value drops below ~0.1 (the typical value for reconnection in the near-Earth solar wind) as the local plasma β increases [*Sonnerup*, 1970; *Slavin and Holzer*, 1979; *Anderson et al.*, 1997; *DiBraccio et al.*, 2013]. If this is so, we would expect the reconnection efficiency at Neptune's magnetopause to be lower than 0.1, due to the high plasma β in Neptune's magnetosheath (see Figure 2f). If we assume an Earth magnetopause-like efficiency of 0.1, then Figure 9 suggests a typical electric field strength at Neptune's magnetopause that is ~0.02 mV m^{-1}; whereas if we assume a lower efficiency of 0.01, then the typical electric field strength would be ~0.002 mV m^{-1}. These values are slightly lower than the model-predicted values for Uranus.

As mentioned at the beginning of this subsection, we can place an upper limit on the reconnection voltage at Neptune. If reconnection occurs at all points along a line on the magnetopause surface (a reconnection "X line") then the reconnection voltage is the potential difference between one end of the line and the other. If we use our most favorable case for reconnection at Neptune's magnetopause shown in Figure 9, and assume that a reconnection X line forms that spans the dayside surface and is ~70 R_N long, then our (more generous) typical

electric field strength of ~0.02 mV m^{-1} suggests an upper limit to the reconnection voltage of ~35 kV. The typical reconnection voltage at Neptune is likely to be significantly lower than this upper limit. Note that this estimated reconnection voltage upper limit for Neptune is similar to that at Uranus. This is because Neptune's magnetosphere is larger, potentially allowing longer X lines that counteract the weaker reconnection electric field.

5. Summary

We have used an analytical modeling approach to investigate how the solar wind interacts with Neptune's magnetosphere via magnetic reconnection at the magnetopause boundary of the system. We have used the same modeling approach as that used by *Masters* [2014] for the case of Uranus, and we have compared the present Neptune results with their Uranus results.

Our modeling suggests that typical near-Neptune solar wind parameters make conditions at Neptune's magnetopause less favorable for magnetic reconnection than at the magnetopause boundary of any other solar system magnetosphere. The location of reconnection sites on Neptune's magnetopause is expected to be highly sensitive to planetary longitude and season as well as the orientation of the IMF, which is comparable to the situation at Uranus. The present Neptune modeling results also indicate a Uranus-like seasonal dependence of magnetopause reconnection, where conditions are more favorable for magnetopause reconnection for one of the dominant IMF orientations than for the other at equinox, whereas at solstice there is symmetry between the two IMF polarities in this respect. We estimate the upper limit of the reconnection voltage applied to Neptune's magnetosphere as 35 kV but point out that the typical voltage is expected to be considerably lower.

A great deal remains to be learned about how the solar wind interacts with the magnetosphere of the outermost planet, and what role the solar wind plays in driving energy flow through Neptune's magnetosphere. Additional means of coupling to the solar wind need to be considered (e.g., via a "viscous-like" interaction), as well as the effectiveness of Triton-related internal mass loading as a competing driver of the system. A mystery that deserves to be highlighted here is the question of why Voyager 2 observations suggest different dynamical states of the magnetospheres of Uranus and Neptune. Solar wind-driven convection, injection-like processes, dynamic whistler mode emissions, and an appreciable radiation belt were identified at Uranus [*Selesnick and McNutt*, 1987; *Mauk et al.*, 1987, 1994; *Kurth and Gurnett*, 1991], unlike at Neptune [*Mauk and Fox*, 2010]. The modest differences between the recent Uranus and present Neptune reconnection assessments do not indicate an answer to this question. The physics of both ice giant magnetosphere is likely to remain mysterious until we continue in situ spacecraft exploration, in the form of planetary orbiters [e.g., *Arridge et al.*, 2014; *Masters et al.*, 2014].

Acknowledgments
Please direct data requests to Adam Masters (a.masters@imperial.ac.uk).

Michael Liemohn thanks the reviewers for their assistance in evaluating this paper.

References

Anderson, B. J., T.-D. Phan, and S. A. Fuselier (1997), Relationships between plasma depletion and subsolar reconnection, *J. Geophys. Res.*, *102*, 9531–9542, doi:10.1029/97JA00173.

Arridge, C. S., et al. (2014), The science case for an orbital mission to Uranus: Exploring the origins and evolution of ice giant planets, *Planet. Space Sci.*, *104*, 122–140.

Bagenal, F. (2013), Planetary magnetospheres, in *Planets, Stars and Stellar Systems*, edited by T. D. Oswalt, L. M. French, and P. Kalas, p. 251, Springer, Dordrecht, Netherlands.

Bagenal, F., J. W. Belcher, E. C. Sittler Jr., and R. P. Lepping Jr. (1987), The Uranian bow shock: Voyager 2 inbound observations of a high Mach number shock, *J. Geophys. Res.*, *92*, 8603–8612, doi:10.1029/JA092iA08p08603.

Belcher, J. W., et al. (1989), Plasma observations near Neptune—Initial results from Voyager 2, *Science*, *246*, 1478–1483.

Cassak, P. A., and A. Otto (2011), Scaling of the magnetic reconnection rate with symmetric shear flow, *Phys. Plasmas*, *18*, 074501, doi:10.1063/1.3609771.

Cassak, P. A., and M. A. Shay (2007), Scaling of asymmetric magnetic reconnection: General theory and collisional simulations, *Phys. Plasmas*, *14*, 102114, doi:10.1063/1.2795630.

Connerney, J. E. P., et al. (1991), The magnetic field of Neptune, *J. Geophys. Res.*, *96*, 19,023–19,042, doi:10.1029/91JA01165.

Decker, R. B., et al. (2008), Mediation of the solar wind termination shock by non-thermal ions, *Science*, *454*, 67–70.

Desch, M. D., et al. (1991), The role of solar wind reconnection in driving the Neptune radio emission, *J. Geophys. Res.*, *96*, 19,111–19,116, doi:10.1029/91JA01138.

DiBraccio, G. A., J. A. Slavin, S. A. Boardsen, B. J. Anderson, H. Korth, T. H. Zurbuchen, J. M. Raines, D. N. Baker, R. L. McNutt Jr., and S. C. Solomon (2013), MESSENGER observations of magnetopause structure and dynamics at Mercury, *J. Geophys. Res. Space Physics*, *118*, 997–1008, doi:10.1002/jgra.50123.

Dungey, J. W. (1961), Interplanetary magnetic field and the auroral zones, *Phys. Rev. Lett.*, *6*, 47–48.

Fuselier, S. A., and W. S. Lewis (2011), Properties of near-Earth magnetic reconnection from in-situ observations, *Space Sci. Rev.*, *160*, 95–121.

Gosling, J. T. (2012), Magnetic reconnection in the solar wind, *Space Sci. Rev.*, *172*, 187–200.

Holme, R., and J. Bloxham (1996), The magnetic fields of Uranus and Neptune: Methods and models, *J. Geophys. Res.*, *101*, 2177–2200, doi:10.1029/95JE03437.

Huddleston, D. E., et al. (1997), Magnetopause structure and the role of reconnection at the outer planets, *J. Geophys. Res.*, *102*, 24,289–24,302, doi:10.1029/97JA02416.
Kobel, E., and E. O. Flückiger (1994), A model of the steady state magnetic field in the magnetosheath, *J. Geophys. Res.*, *99*, 23,617–23,622, doi:10.1029/94JA01778.
Kurth, W. S., and D. A. Gurnett (1991), Plasma waves in planetary magnetospheres, *J. Geophys. Res.*, *96*, 18,977–18,991, doi:10.1029/91JA01819.
Lepping, R. P., et al. (1992), Neptune's polar cusp region—Observations and magnetic field analysis, *J. Geophys. Res.*, *97*, 8135–8144, doi:10.1029/92JA00314.
Masters, A. (2014), Magnetic reconnection at Uranus' magnetopause, *J. Geophys. Res. Space Physics*, *119*, 5520–5538, doi:10.1002/2014JA020077.
Masters, A., et al. (2014), Neptune and Triton: Essential pieces of the solar system puzzle, *Planet. Space Sci.*, *104*, 108–121.
Mauk, B. H., and N. J. Fox (2010), Electron radiation belts of the solar system, *J. Geophys. Res.*, *115*, A12220, doi:10.1029/2010JA015660.
Mauk, B. H., S. M. Krimigis, E. P. Keath, A. F. Cheng, T. P. Armstrong, L. J. Lanzerotti, G. Gloeckler, and D. C. Hamilton (1987), The hot plasma and radiation environment of the Uranian magnetosphere, *J. Geophys. Res.*, *92*(A13), 15,283–15,308, doi:10.1029/JA092iA13p15283.
Mauk, B. H., E. P. Keath, M. Kane, S. M. Krimigis, A. F. Cheng, M. H. Acuña, T. P. Armstrong, and N. F. Ness (1991), The magnetosphere of Neptune: Hot plasmas and energetic particles, *J. Geophys. Res.*, *96*(S01), 19,061–19,084, doi:10.1029/91JA01820.
Mauk, B. H., E. P. Keath, and S. M. Krimigis (1994), Unusual satellite-electron signature within the Uranian magnetosphere and its implications regarding whistler electron loss processes, *J. Geophys. Res.*, *99*(A10), 19,441–19,450, doi:10.1029/94JA01658.
Mozer, F. S., and A. Hull (2010), Scaling the energy conversion rate from magnetic field reconnection to different bodies, *Phys. Plasmas*, *17*, 102906, doi:10.1063/1.3504224.
Ness, N. F., et al. (1989), Magnetic fields at Neptune, *Science*, *246*, 1473–1478.
Parker, E. N. (1958), Dynamics of the interplanetary gas and magnetic fields, *Astrophys. J.*, *128*, 664–676.
Paschmann, G., et al. (2013), In situ observations of reconnection in space, *Space Sci. Rev.*, *178*, 385–417.
Petrinec, S. M., and C. T. Russell (1997), Hydrodynamic and MHD equations across the bow shock and along the surfaces of planetary obstacles, *Space Sci. Rev.*, *79*, 757–791.
Petrinec, S. M., et al. (1997), Geotail observations of magnetosheath flow near the magnetopause, using Wind as a solar wind monitor, *J. Geophys. Res.*, *102*, 26,943–26,959, doi:10.1029/97JA01637.
Petrinec, S. M., et al. (2003), Steady reconnection during intervals of northward IMF: Implications for magnetosheath properties, *J. Geophys. Res.*, *108*(A12, 1458), doi:10.1029/2003JA009979.
Phan, T. D., T. E. Love, J. T. Gosling, G. Paschmann, J. P. Eastwood, M. Oieroset, V. Angelopoulos, J. P. McFadden, D. Larson, and U. Auster (2011), Triggering of magnetic reconnection in a magnetosheath current sheet due to compression against the magnetopause, *Geophys. Res. Lett.*, *38*, L17101, doi:10.1029/2011GL048586.
Phan, T. D., G. Paschmann, J. T. Gosling, M. Oieroset, M. Fujimoto, J. F. Drake, and V. Angelopoulos (2013), The dependence of magnetic reconnection on plasma β and magnetic shear: Evidence from magnetopause observations, *Geophys. Res. Lett.*, *40*, 11–16, doi:10.1029/2012GL054528.
Phan, T.-D., et al. (2010), The dependence of magnetic reconnection on plasma β and magnetic shear: Evidence from solar wind observations, *Astrophys. J., Lett.*, *719*, L199–L203.
Richardson, J. D. (1993), A quantitative model of plasma in Neptune's magnetosphere, *Geophys. Res. Lett.*, *20*, 1467–1470, doi:10.1029/93GL01353.
Richardson, J. D., and R. L. McNutt (1990), Low-energy plasma in Neptune's magnetosphere, *Geophys. Res. Lett.*, *17*, 1689–1692, doi:10.1029/GL017i010p01689.
Richardson, J. D., J. W. Belcher, M. Zhang, and R. L. McNutt Jr. (1991), Low-energy ions near Neptune, *J. Geophys. Res.*, *96*, 18,993–19,011, doi:10.1029/91JA01598.
Sanny, J., R. L. McPherron, C. T. Russell, D. N. Baker, T. I. Pulkkinen, and A. Nishida (1994), Growth-phase thinning of the near-Earth current sheet during the CDAW 6 substorm, *J. Geophys. Res.*, *99*(A4), 5805–5816, doi:10.1029/93JA03235.
Selesnick, R. S. (1990), Plasma convection in Neptune's magnetosphere, *Geophys. Res. Lett.*, *17*, 1681–1684, doi:10.1029/GL017i010p01681.
Selesnick, R. S., and R. L. McNutt Jr. (1987), Voyager 2 plasma ion observations in the magnetosphere of Uranus, *J. Geophys. Res.*, *92*, 15,249–15,262, doi:10.1029/JA092iA13p15249.
Slavin, J. A., and R. E. Holzer (1979), The effect of erosion on the solar wind stand-off distance at Mercury, *J. Geophys. Res.*, *84*, 2076–2082, doi:10.1029/JA084iA05p02076.
Slavin, J. A., and R. E. Holzer (1981), Solar wind flow about the terrestrial planets: 1. Modeling bow shock position and shape, *J. Geophys. Res.*, *86*, 11,401–11,418, doi:10.1029/JA086iA13p11401.
Sonnerup, B. U. O. (1970), Magnetic field reconnection in a highly conducting incompressible fluid, *J. Plasma Phys.*, *4*, 161–174.
Stone, E. C., and E. D. Miner (1989), The Voyager 2 encounter with the Neptunian system, *Science*, *246*, 1417–1421.
Swisdak, M., and J. F. Drake (2007), Orientation of the reconnection X-line, *Geophys. Res. Lett.*, *34*, L11106, doi:10.1029/2007GL029815.
Swisdak, M., B. N. Rogers, J. F. Drake, and M. A. Shay (2003), Diamagnetic suppression of component magnetic reconnection at the magnetopause, *J. Geophys. Res.*, *108*(A5), 1218, doi:10.1029/2002JA009726.
Swisdak, M., M. Opher, J. F. Drake, and F. Alouani Bibi (2010), The vector direction of the interstellar magnetic field outside the heliosphere, *Astrophys. J.*, *710*, 1769–1775.
Szabo, A., and R. P. Lepping (1995), Neptune inbound bow shock, *J. Geophys. Res.*, *100*, 1723–1730, doi:10.1029/94JA02491.
Szabo, A., G. L. Siscoe, A. J. Lazarus, R. L. McNutt Jr., R. P. Lepping, and N. F. Ness (1991), Magnetopause and cusp observations at Neptune, *J. Geophys. Res.*, *96*(S01), 19,149–19,152, doi:10.1029/91JA01600.
Voigt, G.-H., and N. F. Ness (1990), The magnetosphere of Neptune—Its response to daily rotation, *Geophys. Res. Lett.*, *17*, 1705–1708, doi:10.1029/GL017i010p01705.
Zhang, M., J. D. Richardson, and E. C. Sittler Jr. (1991), Voyager 2 electron observations in the magnetosphere of Neptune, *J. Geophys. Res.*, *96*(S01), 19,085–19,100, doi:10.1029/91JA01857.
Zwan, B. J., and R. A. Wolf (1976), Depletion of solar wind plasma near a planetary boundary, *J. Geophys. Res.*, *81*, 1636–1648, doi:10.1029/JA081i010p01636.